CONNECTING THE SUN AND THE SOLAR WIND:
I. SOURCE REGIONS OF THE FAST WIND OBSERVED BEYOND 0.3 AU

Richard Woo

Jet Propulsion Laboratory, California Institute of Technology, 4800 Oak Grove Drive,
Pasadena, CA 91109

Shadia Rifai Habbal

Harvard-Smithsonian Center for Astrophysics, 60 Garden Street, Cambridge, MA 02138

ABSTRACT

Radio occultation and white-light measurements have shown that the solar corona comprises three distinct morphological regions in path-integrated density: streamer, quiet Sun, and polar coronal hole. Using solar wind flow speeds inferred from O VI lines with the ultraviolet coronagraph spectrometer (UVCS) on the Solar and Heliospheric Observatory (SOHO) and polarized brightness (pB) measurements of path-integrated density by the High Altitude Observatory (HAO) Mauna Loa Mk III K-coronameter made at the same time, this study shows that the latitudinal flow speed profile reflects the same three regions identified in the latitudinal profile of density. The streamer region of angular extent about 46° includes the streamer stalk, which encompasses the heliospheric current sheet in interplanetary space and carries the slowest wind. Flow speed rises steadily with increasing distance from the stalk, reaching high speed in the quiet Sun region and peaking in the polar coronal hole region. These results enable the Mk III K-coronameter pB measurements at 1.15 and 1.74 Ro to serve as a proxy for the distribution of flow speed in both the inner and outer corona, thus connecting the Sun and the solar wind. We use this framework to demonstrate that the fast wind regions observed beyond 0.3 AU map radially into the fast wind regions observed at the Sun.

1. Introduction

Since the existence of the solar wind was confirmed directly by Mariner 2 in 1962 [*Neugebauer and Snyder*, 1966], connecting the Sun and the solar wind has been one of the primary goals of solar wind research. As the number of interplanetary spacecraft has grown, so has our knowledge and understanding of the morphology of the three-dimensional heliosphere beyond 0.3 AU. By comparison, definitive measurements of the spatial distribution of plasma parameters in the solar corona have been very rare.

Coronal holes have been regarded as the sources of the high speed streams observed by interplanetary spacecraft for over twenty years [*Zirker*, 1977; *Hundhausen*, 1977]. When direct high latitude measurements were eventually made by the Ulysses mission, it was further concluded that the observed fast wind at high latitude emanated solely from polar coronal holes and that it expanded superradially [e.g., *Gosling et al.*, 1995; *Neugebauer*, 1999]. These major conclusions about the solar sources of the fast solar wind were not established by comparing the solar wind measurements with velocity or magnetic field measurements in the corona, because none were available. Instead, the only observational connection was made by extrapolating the in situ velocity measurements made beyond 0.3 AU back to the sun, and associating them with coronal holes deduced from soft X-ray or He I 1083 nm measurements and white-light images of the corona (*Kreiger et al.*, 1973; *Munro and Jackson*, 1977; *Bame et al.*, 1993; *Gosling et al.*, 1995).

Fundamental information on the morphology of coronal density has now emerged as a result of highly sensitive radio occultation and white-light measurements of the tenuous outer corona [*Woo and Habbal*, 1999a,b]. By comparing the latitudinal density (hereafter we will use density to mean path-integrated density) profiles of the inner and outer corona, it has been possible to follow the evolution of polar coronal holes and demonstrate that polar coronal holes expand radially rather than superradially as previously thought [*Munro and Jackson*, 1977]. Furthermore, it has been shown that polar coronal holes, the quiet Sun and streamers comprise the three distinct morphological regions of coronal density near solar minimum. Density in the quiet Sun region is a factor of 2–3 higher than that of the polar coronal hole, but the latitudinal density profile of both quiet Sun and polar coronal hole regions is radially preserved. The streamer region encompasses the heliospheric current sheet that evolves from coronal streamers within a few solar radii of the Sun. It is defined as the region in which the latitudinal density profile of the outer corona beyond 5 Ro no longer matches the radially preserved density profile of the inner corona at 1.15 Ro. Instead, the latitudinal gradient rises steeply as it departs from a radial expansion.

New flow speed measurements of the corona have also been made. Radio occultation (mainly IPS for interplanetary scintillation) measurements have probed solar wind velocity in the solar corona for many years [*Ekers and Little*, 1971; *Armstrong et al.*, 1986; *Grall et al.*, 1996], and hinted at the source regions of the solar wind [*Woo*, 1995; *Woo and Martin* 1997]. However, it remained for ultraviolet Doppler dimming measurements to provide the definitive measurements of latitudinal variation, because, unlike the radio measurements, they were able to map a significant portion of the plane of the sky essentially at the same time [*Habbal et al.*, 1997]. These measurements confirmed that streamer stalks are the sources of the slowest solar wind, and that the fast wind pervades the inner corona. (For reviews of the recent developments in both density and flow speed measurements of the solar corona, see *Woo and Habbal* [1998, 1999c] and references therein).

In this paper, we build on the recent observational results for density and flow speed by comparing simultaneous measurements of both. By showing that flow speed reflects the same three morphological regions observed in density, we demonstrate that density also acts as a proxy for flow speed at the Sun. The HAO Mauna Loa Mk III K-coronameter has been routinely providing invaluable density measurements of the corona since 1980 [*Fisher et al.*, 1981, 1982]. Although reliable measurements are limited to the inner corona, information on the outer corona is also obtained as a result of the gains in our knowledge of coronal morphology from this and previous work. Mk III, therefore, provides the heretofore missing framework of measurements of density and flow speed in both the inner and outer corona with which connections to solar wind measurements can be made. We begin our study of these connections by investigating the source regions of the fast solar wind observed beyond 0.3 AU.

2. Simultaneous Density and Flow Speed Measurements in the Solar Corona

2.1 Solar Wind Flow Speed

For solar wind flow speed, we use the profiles obtained by *Habbal et al.* [1997] using the ultraviolet coronagraph spectrometer (UVCS) on board the Solar and Heliospheric Observatory (SOHO) [*Kohl et al.*, 1997] in this study. Reproduced in Plates 1a and 2a are the UVCS measurements of January 17–19, 1997 and April 23–27, 1997, respectively. The white-light images providing coronal context were taken with the SOHO LASCO (for Large Angle Spectrograph Coronagraph) C2 coronagraph [*Brueckner et al.*, 1997] on January 17 (Plate 1a) and April 27 (Plate 2a). The solid white line contours in each image trace the locations where the ratio of the oxygen 1032/1037 intensities measured by UVCS was equal to two, or equivalently where the flow speed was 94 km s^{-1}. The radial distances of these contours in terms of position angle (latitude measured counterclockwise with respect to ecliptic north) are plotted in Plates 1b–1d and Plates 2b–2d, with radial distance increasing downwards along the y-axis to depict a corresponding flow speed that increases along the y-axis. The measurement uncertainty in the position of the white line contours is ±0.05 Ro in radial distance and ±3° in latitude.

2.2 Density

For density during the UVCS measurements, we use the pB measurements made by the HAO Mauna Loa Mk III K-coronameter white-light measurements [*Fisher et al.*, 1981]. (Because of the location of the pylon holder, in the southeast quadrant [*Brueckner et al.*, 1995], we could not use the LASCO measurements). In the remainder of this paper, profile denotes latitudinal profile, inner corona corresponds to 1.15 Ro and outer corona to that beyond 5 Ro. Both inner and outer corona profiles are needed to demarcate the streamer, polar coronal hole, and quiet Sun regions. We will describe each separately.

2.2.1 Inner corona density profile

The Mk III pB profiles at 1.15 Ro have been added to Plates 1b and 2b. The January 19 (April 27) profile in Plate 1b (Plate 2b) is closest in time to the UVCS measurements of the southern (northern) hemisphere. The two (one) vertical lines designated II and III in Plate 1b (III in Plate 2b) represent the radial extensions of the coronal hole boundaries, as defined by the He I 1083 nm solar disk maps of the National Solar Observatory. These boundaries are shown as dashed white lines in Plate 1a (Plate 2b), demarcating the coronal hole and neighboring quiet Sun regions. The pB profile at 1.15 Ro increases by a factor of 2–3 from polar coronal hole to quiet Sun, as is generally the case [*Woo and Habbal*, 1999b]. Radially preserved, this inner corona profile defines the outer corona profile except for the streamer region discussed below.

2.2.2 Outer corona density profile

The boundaries of the streamer region encompassing the streamer stalk are defined by the density profile of the outer corona. Inside the streamer region, the density profile of the outer corona no longer matches the radially preserved density profile of the inner corona [*Woo and Habbal*, 1999b]. For this reason, demarcation between the quiet Sun and streamer region (indicated by the dashed white lines marked I and IV in Plate 1a and I and II in Plate 2a) requires measurements of both the inner and outer corona. Determining the streamer boundary is, therefore, more involved than determining the boundaries of the coronal hole region, which can be carried out with either the 1.15 Ro profiles or the He I 1083 nm maps.

The Mk III pB profiles at 1.74 Ro are shown in Plate 1c (Plate 2c). We have selected the January 18 profile for the east limb and the January 21 (April 27) profile for the west limb because these best match the times of the UVCS measurements. Mk III observes the corona at higher altitudes, but we choose to use the profiles at 1.74 Ro because this is the highest altitude before which detection of density near the boundaries of the streamer region may become a problem due to reduced measurement sensitivity. The sharp increase in the gradient of the radial distance profile near position angle 140° in Plate 1c, indicating a steep drop in flow speed, suggests that it corresponds to boundary I, the end of the quiet Sun region and the start of the streamer region. The vertical line on the 1.74 Ro profile of Plate 1c has been drawn at this location and labelled I; it crosses the steep pB profile that is anti-correlated with the profile of flow speed at a level of about 100×10^{-10} Bo (represented by the horizontal line).

To reinforce the pB level that can be used as a proxy for the streamer boundary, we compared the pB profile of August 11, 1997 at 1.74 Ro with the density profiles at 1.15 and 5.5 Ro investigated in *Woo and Habbal* [1999b]. Departure between the 1.15 and 5.5 Ro profiles occurred where the pB level at 1.74 Ro was 100×10^{-10} Bo on the east limb and where pB was 70×10^{-10} Bo on the west limb. Hence, we assume that the pB level of 100×10^{-10} Bo in the 1.74 Ro profile is a relatively good indicator of the location of the demarcation between the quiet Sun and the streamer region. We emphasize that the 1.74 Ro profile is being used here as a proxy for the outer corona profile.

2.3 Density as a Proxy for Flow Speed

There is remarkable consistency in the relationship between the latitudinal profiles of density and flow speed displayed in Plates 1 and 2. Density and flow speed at the Sun are in general anticorrelated, with the flow speed profiles reflecting the same three major morphological regions of the corona observed in the density measurements. Density is lowest, and the solar wind fastest, in the polar coronal hole. Beyond the polar coronal hole and in the quiet Sun region where density rises by a factor of about 2–3, flow speed is still fast, but it is unmistakably lower than that emanating from the coronal hole. Within the streamer region of angular extent about 46°, there is a steady increase in density and a steady decrease in velocity with decreasing angular distance from the streamer stalk. That the morphology of flow speed reflects that of density means that measurements of density also serve as a proxy for solar wind velocity.

One difference between the density and radial distance (and consequently flow speed) profiles in Plates 1b–d and 2b–d is that the density profiles are for a fixed altitude, while the flow speed profiles are not. Still, if the inverse distance is taken as an indicator of flow speed, then flow speed in the quiet Sun region is not more than 25% slower than that in the coronal hole, while in the streamer region it is as much as 65% lower.

As we have seen, fast wind prevails outside the streamer region, i.e., within the polar coronal hole and quiet Sun regions. By showing that the boundary between the quiet Sun and streamer region corresponds approximately to the level of 100×10^{-10} Bo in the Mk III K-coronameter measurements of pB at 1.74 Ro, we have essentially determined a criterion for identifying the fast wind regions at the Sun in these measurements. Since the Mauna Loa K-coronameter has been imaging the solar corona almost continuously since 1980 (*Fisher et al.*, 1982), the Mk III measurements represent an invaluable coronal data base with which connections to solar wind measurements beyond 0.3 AU can be established.

3. Connecting Fast Solar Wind Observed Beyond 0.3 AU to the Sun

To connect the distribution of fast wind observed in situ beyond 0.3 AU (the closest distance these measurements have been made) to the Sun, we use the pB criterion and compare it with velocity maps. Since the pB measurements are in the plane of the sky and are made daily, synoptic (latitude-longitude) pB maps can be readily compared with synoptic solar wind maps. The latter maps have been constructed by *Crooker et al.* [1997] and *Neugebauer et al.* [1998] from solar wind flow speed measurements by Ulysses during its rapid latitude scan in 1995 near 1.34 AU and on low latitude measurements by Wind at 1 AU.

Reproduced in Plate 3 is the map from *Neugebauer et al.* [1998] covering Carrington rotations CR 1891–1895 with the synoptic contour maps of pB based on the Mk III K-coronameter measurements at 1.74 Ro superimposed on them. Two different rotations — CR 1893 based on east limb data (Plate 3a), and CR 1893 based on east limb data (Plate 3b) — are shown to illustrate the temporal change observed during the Ulysses measurements. As seen earlier, the pB = 100×10^{-10} Bo contour defines the streamer/quiet Sun boundary, hence the low-latitude boundary of the fast wind. It should be compared with the 700 km/s contour of solar wind measurements. Despite the use of pB as a proxy for velocity, the differences between point and global path-integrated density measurements and their longitudinal probing locations, the assumptions in extrapolation of the solar wind measurements back to the Sun, the evolution of the solar wind with radial distance, and temporal variations during the five solar rotations, the similarity in shape and location between these two contours representing solar corona and solar wind is striking. There is better agreement between the pB and solar wind measurements in the southern hemisphere in Plate 4b, especially in the longitude range of 180°–360°, because the time of CR 1891 was closer to that when Ulysses probed the southern hemisphere. The remarkable coincidence between the solar corona and solar wind boundaries means that the fast solar wind regions observed by Ulysses map radially into the fast wind regions at the Sun.

Latitude-longitude maps of the contours of flow speed have also been deduced from IPS measurements made by the Nagoya network of radio telescopes [*Kojima et al.* 1998] in the distance range of 0.3–1.0 AU. Shown in Plate 4a are the Nagoya maps for CR 1857–1858 and in Plate 4b those for CR 1912. These maps show significant changes in the regions of the fast solar wind over the period of four years (1992–1996) during the declining phase of the solar cycle. Superimposed respectively on these are the Mk III latitude-longitude maps of pB at 1.74 Ro for CR 1857 based on west limb data, and for CR 1912 based on east limb data.

The coincidence between the 700 km/s boundaries and the Mk III pB = 100 x 10^{-10} Bo contours in Plate 4 is even more remarkable than that in Plate 3, probably reflecting the fact that IPS and white-light both observe the solar wind off the limb of the Sun, that the IPS observations are closer to the Sun than those by Ulysses, and that the observations in Plate 4 cover a period shorter than those in Plate 3 so that temporal variations are less significant. In the case of CR 1857–1858 (Plate 4a), there is notable discrepancy between the pB and Ulysses contours in the longitudinal range of 60-210° near latitude –45°. This may be caused by temporal change, since source surface magnetic field maps [*Hoeksema and Scherrer*, 1986] show considerable change in this region between CR 1856 and CR 1857.

As concluded by *Habbal et al.* [1997], and evident within the streamer region of angular extent about 46° in Plates 1 and 2, the source of the slowest solar wind is the streamer stalk, with flow speed steadily rising with increasing angular distance from it. On the other hand, in situ solar wind measurements near the ecliptic plane have shown profiles of flow speed as a function of latitudinal separation from the heliospheric current sheet that are similar in shape and angular extent [*Hakamada and Akasofu*, 1981; *Zhao and Hundhausen*, 1981; *Newkirk and Fisk*, 1985; *Bruno et al.*, 1986; *Kojima and Kakinuma*, 1990]. This similarity is not surprising since Faraday rotation observations have shown that the streamer stalk encompasses the heliospheric current sheet in the corona [*Woo*, 1997]. The results in Plate 3, however, give more details of this connection.

Neugebauer et al. [1998] pointed out that the band of low speed solar wind along the heliospheric current sheet in the Ulysses solar wind measurements displayed in Plate 3 is not uniform. The solar wind evolves with heliocentric distance, as evidenced by the formation of interaction regions, and suggested by the fact that the heliospheric current sheet observed by Ulysses no longer coincides with the lowest speed wind [*Crooker et al.*, 1997; *Neugebauer et al.*, 1998]. However, the results in Plate 3 strongly suggest that the non-uniformity of the low-speed solar wind along the heliospheric current sheet observed by Ulysses has its origin at the Sun. Despite representing path-integrated measurements, the 1.74 Ro profiles in Plate 3 are able to clearly discern two regions of enhanced density (and, by proxy, depressed flow speed) at the Sun, and these roughly coincide with the two regions of lowest speed flow observed by Ulysses beyond 1 AU. The anticorrelation between coronal density and solar wind speed measurements at latitudes lower than 60° has also been identified in other studies based on IPS measurements near solar minimum [*Sime and Rickett*, 1981; *Yokobe et al.*, 1999]. Thus, not only does the boundary of the fast wind (streamer region) extend approximately radially into interplanetary space, so apparently do the islands of the slowest solar wind which also correspond to the brightest streamer stalks encompassing the heliospheric current sheet.

4. Conclusions and Discussion

Building on earlier results on the morphology of density from radio occultation and white-light measurements, and the morphology of solar wind flow speed in the corona from ultraviolet Doppler dimming measurements, we have compared simultaneous white-light and ultraviolet measurements made in 1997. During this time, the three major morphological regions of the corona — polar coronal hole, quiet Sun, and coronal streamer — were most isolated from each other in path-integrated (pB and Doppler dimming) measurements because the heliospheric current sheet was relatively flat. Taking advantage of this configuration, and determining the boundaries from the latitudinal profiles rather than visual inspection of the images, we have shown that flow speed at the Sun is anticorrelated with density, and that its latitudinal variation reflects that of coronal density. The streamer region of angular extent about 46° includes the streamer stalk, which encompasses the heliospheric current sheet and carries the slowest wind. Flow speed rises steadily with increasing distance from the streamer stalk, reaching high speed in the quiet Sun region and peaking in the polar coronal hole region. Based merely on density measurements without invoking any modeling, these results indicate that while polar coronal holes produce the fastest wind, they are not special as sources of the fast wind.

Besides defining the relationship between density and flow speed at the Sun, the results of this paper demonstrate that white-light measurements make available not only information on the three-dimensional distribution of density in the near-Sun solar wind, but also serve as a proxy for solar wind velocity. The pB measurements by the HAO Mauna Loa Mk III K-coronameter have imaged the corona essentially continuously since 1980. Although limited to reliable measurements close to the Sun, we have shown in this paper how the Mk III 1.74 Ro profiles serve also as a proxy for profiles of the outer corona and define the regions of the fast wind by demarcating the streamer from the coronal hole and quiet Sun regions. On the other hand, previous work showed that the Mk III 1.15 Ro profiles define the distribution of density (and indirectly flow speed) in the outer corona of both polar coronal hole and quiet Sun regions [*Woo and Habbal*, 1999a,b]. The Mk III measurements at 1.15 and 1.74 Ro, therefore, provide the previously unavailable framework of density and flow speed measurements of the inner and outer corona necessary for connecting the Sun and solar wind.

We have used this newfound framework to identify the global fast wind regions in latitude-longitude maps of coronal density, and compared them with corresponding maps of the fast wind regions observed by both IPS and Ulysses beyond 0.3 AU. The similarity of these two widely separated regions in several significantly different fast wind cases demonstrates that the fast wind does not expand superradially between Sun and Earth, thus reinforcing what had already been concluded from coronal measurements alone [*Woo and Habbal*, 1999a,b].

Interestingly enough, when *Schwenn et al.* [1978] compared white light measurements at 1.5 Ro with Helios flow speed measurements, they found close correlations between the latitudinal boundaries of fast wind and coronal holes, prompting them to conclude that there was only minor nonradial expansion in latitude beyond 1.5 Ro, and pointing out that this was in contradiction with the conclusions of *Munro and Jackson* [1977]. The Helios results are very similar to those of this paper if it is recognized that: (1) the contour identified previously as the polar coronal hole boundary in the white-light measurements at 1.5 Ro is actually the boundary of the streamer region, and (2) the corona in the polar coronal hole and quiet Sun regions expands radially between 1.15 and 1.5 Ro.

Comparisons between white-light and Ulysses solar wind measurements of the streamer region also suggest that the non-uniformity of the slowest solar wind along the heliospheric current sheet observed by Ulysses has its origin at the Sun. The islands of enhanced density at the Sun (representing the brightest streamer stalks) remain the sources of the slowest solar wind along the heliospheric current sheet. Away from these islands, however, peaks in density are lower and minima in flow speed are higher, as evident in the Ulysses solar wind measurements beyond 1 AU. Taking into account the non-uniformity of peak density and minimum flow speed along the heliospheric current sheet should improve models of the solar wind in which wind speeds are assumed to depend only on the angular distance from the heliospheric current sheet [*Wang et al.*, 1997], as evident in the flow speed profiles of Plates 1–2.

Evidence for a radially expanding solar wind was first found in radio occultation measurements of the corona, then in global imaging white-light measurements of the corona, and now in solar wind measurements beyond 0.3 AU. Clearly, coronal measurements provide the most compelling evidence, since they take place closest to the source regions and before the solar wind evolves. The evidence from solar wind measurements far from the Sun is, however, also significant, because previous investigations based on such measurements either assumed or reached the opposite conclusion of this paper, that fast solar wind originates exclusively from coronal holes and that polar coronal holes expand superradially producing high speed streams near the solar equator [e.g., *Hundhausen*, 1977; *Sime and Rickett*, 1978; *Kojima and Kakinuma*, 1990; *Rickett and Coles*, 1991; *Bame et al.*, 1993; *Gosling et al.*, 1995; *Coles*, 1995;*Wang et al.*, 1997; *Woch et al.*, 1997; *Neugebauer*, 1999]. Although a discussion of these studies is beyond the scope of this paper, it should be pointed out that our investigation is very different because it is based entirely on observations and does not rely on theoretical modeling. Most importantly, the observations include coronal measurements sensitive enough to define the latitudinal density profiles in the highly tenuous outer corona and coronal flow speed measurements that show the anticorrelation between flow speed and density.

Acknowledgments. We thank C. Copeland for expertly producing the plates of this paper, H. Gilbert and A. Lecinski for many useful discussions and for generously providing the Mauna Loa Mk III K-coronameter (operated by NCAR/HAO) data, R. Howard (NRL) for the LASCO images, J. Kohl for the UVCS data, M. Kojima for providing the Nagoya IPS maps and discussion, and M. Neugebauer for providing the original of the Ulysses solar wind speed map. The NSO/Kitt Peak He I 1083 nm data used here were produced cooperatively by NSF/NOAO, NASA/GSFC, and NOAA/SEL. This paper describes research carried out at the Jet Propulsion Laboratory, California Institute of Technology, under a contract with the National Aeronautics and Space Administration. Support for S.R. Habbal was provided by NASA grant NAG5-6215.

REFERENCES

Armstrong, J.W., W.A. Coles, M. Kojima, and B.J. Rickett, Solar wind observations near the Sun, in *The Sun and the Heliosphere in Three Dimensions*, ed. R.G. Marsden, 59–64, D. Reidel, Dordrecht, Holland, 1986.

Bame, S.J., B.E. Goldstein, J.T. Gosling, J.W. Harvey, D.J. McComas, M. Neugebauer, and J.L. Phillips, Ulysses observations of a recurrent high speed solar wind stream and the heliomagnetic streamer belt, *Geophys. Res. Lett.*, *20*, 2323–2326, 1993.

Brueckner, G.E., R.A. Howard, M.J. Koomen, C.M. Korendykje, D.J. Michels, J.D. Moses, D.G. Socker, K.P. Dere, P.L. Lamy, A. Llebaria, M.V. Bout, R. Schwenn, G.M. Simnett, D.K. Bedford, and C.J. Eyles, The large angle spectroscopic coronagraph (LASCO), *Solar Phys.*, *162*, 357–402, 1995.

Bruno, R., U. Villante, B. Bavassano, R. Schwenn, and F. Mariani, In-situ observations of the latitudinal gradients of the solar wind parameters during 1976 and 1977, *Solar Phys.*, *104*, 431–445, 1986.

Coles, W.A., Interplanetary scintillation observations of the high-latitude solar wind, *Space Sci. Rev.*, *72*, 211–222, 1995.

Crooker, N.U., A.J. Lazarus, J.L. Phillips, J.T. Steinberg, A. Szabo, R.P. Lepping, and E.J. Smith, Coronal streamer belt asymmetries and seasonal solar wind variations deduced from Wind and Ulysses data, *J. Geophys. Res.*, *102*, 4673–4679, 1997.

Ekers, R.D., and L.T. Little, The motion of the solar wind close to the Sun, *Astron. Astrophys.*, *10*, 310–316, 1971.

Fisher, R., R.H. Lee, R.M. MacQueen, and A.I. Poland, New Mauna Loa coronagraph systems, *Appl. Opt.*, *20*, 1094, 1981.

Fisher, R., C. Garcia, K. Rock, P. Seagraves, and E. Yasukawa, The white light solar corona An atlas of K-coronameter synoptic charts August 1980 – September 1981, *NCAR/TN-199+STR*, 1982.

Gosling, J.T., S.J. Bame, W.C. Feldman, D.J. McComas, J.L. Phillips, B. Goldstein, M. Neubebauer, J. Burkepile, A.J. Hundhausen, and L. Acton, The band of solar variability at low heliographic latitudes near solar activity minimum: Plasma results from the Ulysses rapid latitude scan, *Geophys. Res. Lett.*, *22*, 3329–3332, 1995.

Grall, R.R., W.A. Coles, M.T. Klinglesmith, A.R. Breen, P.J.S. Williams, J. Markkanen, and R. Esser, Rapid acceleration of the polar solar wind, *Nature*, *379*, 429–432, 1996.

Habbal, S.R., R. Woo, S. Fineschi, R. O'Neal, J. Kohl, G. Noci, and C. Korendyke, Origins of the slow and the ubiquitous fast solar wind, *Astrophys. J.*, *489*, L103–L106, 1997.

Hakamada, K., and S.I. Akasofu, A cause of solar wind speed variations observed at 1 AU, *J. Geophys. Res.*, *86*, 1290–1298, 1981.

Hoeksema, J.T., and P.H. Scherrer, The solar magnetic field — 1976 through 1985, *Rep. UAG–94*, World Data Cent. A for Sol. Terr. Phys., Boulder, Colo., 1986.

Hundhausen, A.J., An interplanetary view of coronal holes, in *Coronal Holes and High Speed Streams*, ed. J.B. Zirker, 225–329, Colorado Associated University Press, Colorado, 1977.

Kohl, J., R. Esser, L.D. Gardner, S. Habbal, P.S. Daigneau, E.F. Dennis, G.U. Nystrom, A. Panasyuk, J.C. Raymond, P.L. Smith, L. Strachan, A.A. Van Ballegooijen, G. Noci, S. Fineschi, M. Romoli, A. Ciaravella, A. Modigliani, M.C.E. Huber, E. Antonucci, C. Benna, S. Giordano, G. Tondella, P. Nicolosi, G. Naletto, C. Perenechele, D. Spadaro, G. Poletto, S. Livi, O. von. der Lühe, J. Geiss, J.G. Timothy, G. Gloeckler, A. Allegra, G. Basile, R. Brusa, B. Wood, O.H.W. Siegmund, W. Fowler, R. Fisher, and M. Jhabvala, The ultraviolet coronagraph spectrometer for the solar and heliospheric obserevatory, *Sol. Phys.*, *162*, 313–356, 1995.

Kojima, M., and T. Kakinuma, Solar cycle dependence of global distribution of solar wind speed, *Space Sci. Rev.*, *53*, 173–222, 1990.

Kojima, M., M. Tokumaru, H. Watanabe, A. Yokobe, K. Asai, B.V. Jackson, and P.L. Hick, Heliospheric tomography using interplanetary scintillation observations, 2. Latitude and heliocentric distance dependence of solar wind structure at 0.1–1 AU, *J. Geophys. Res.*, *103*, 1981–1989, 1998.

Krieger, A.S., A.F. Timothy, and E.C. Roelof, A coronal hole and its identification as the source of a high velocity solar wind stream, *Solar Phys.*, *23*, 123, 1973.

Munro, R.H., and B.V. Jackson, Physical properties of a polar coronal hole from 2 to 5 Ro, *Astrophys. J.*, *213*, 874–886, 1977.

Neugebauer, M., and C.W. Snyder, Mariner 2 observations of the solar wind 1. Average properties, *J. Geophys. Res.*, *71*, 4469, 1966.

Neugebauer, M., The three-dimensional solar wind at solar activity minimum, *Rev. Geophys.*, *37*, 107–126, 1999.

Neugebauer, M., R.J. Forsyth, A.B. Galvin, K.L. Harvey, J.T. Hoeksema, A.J. Lazarus, R.P. Lepping, J.A. Linker, Z. Mikic, J.T. Steinberg, R. von Steiger, Y.-M. Wang, and R.F. Wimmer-schweingruber, Spatial structure of the solar wind and comparisons with solar data and models, *J. Geophys. Res.*, *103*, 14587–14599, 1998.

Newkirk, G., Jr., and L.A. Fisk. Variation of cosmic rays and solar wind properties with respect to the heliospheric current sheet. 1. Five-GeV protons and solar wind speed, *J. Geophys. Res.*, *90*, 3391, 1985.

Rickett, B.J. , and W.A. Coles, Evolution of the solar wind structure over a solar cycle: Interplanetary scintillation velocity measurements compared with coronal observations, *J. Geophys. Res.*, *96*, 1717–1736, 1991.

Schwenn, R., M.D. Montgomery, H. Rosenbauer, H. Miggenrieder, K.H. Mühlhäser, S.J. Bame, W.C. Feldman, and R.T. Hansen, Direct observation of the latitudinal extent of a high-speed stream in the solar wind, *J. Geophys. Res.*, *83*, 1011–1017, 1978.

Sime, D.G., and B.J. Rickett, The latitude and longitude structure of the solar wind speed from IPS observations, *J. Geophys. Res.*, *83*, 5757-5762, 1978.

Sime, D.G., and B.J. Rickett, Coronal density and the solar wind speed at all latitudes, *J. Geophys. Res.*, *86*, 8869–8876, 1981.

Wang, Y.-M, N.R. Sheeley, Jr., J.L. Phillips, and B.E. Goldstein, Solar wind stream interactions and the wind speed-expansion factor relationship, *Astrophys. J.*, *488*, L51–54, 1997.

Woch, J., W.I. Axford, B. Wilken, S.Livi, J. Geiss, G. Gloeckler, and R.J. Forsyth, SWICS/Ulysses observations: The three-dimensional structure of the heliosphere in the declining/minimum phase of the solar cycle, *Geophys. Res. Lett.*, *24*, 2885–2888, 1997.

Woo, R., Solar wind speed structure in the inner corona at 3–12 Ro, *Geophys. Res. Lett.*, *22*, 1393–1396, 1995.

Woo, R., Evidence for the reversal of magnetic field polarity in coronal streamers, *Geophys. Res. Lett.*, *24*, 97–100, 1997.

Woo, R., and S.R. Habbal, Multiscale filamentary structures in the solar corona and their implications for the origin and evolution of the solar wind, in *Physics of Space Plasmas (1998). Number 15*, eds. T. Chang and J.R. Jasperse, MIT Center for Theoretical Geo/Cosmo Plasma Physics, Cambridge, MA, 351–355, 1998.

Woo, R., and S.R. Habbal, Imprint of the sun on the solar wind, *Astrophys. J.*, *510*, L69–L72, 1999a.

Woo, R., and S.R. Habbal, Radial evolution of density structure in the solar corona, *Geophys. Res. Lett.*, *26*, 1793–1796, 1999b.

Woo, R., and S.R. Habbal, A new view of the origin of the solar wind, in *Solar Wind Nine*, eds. S.R. Habbal, R. Esser, J.V. Hollweg, and P. Isenberg, 71–76, AIP, New York, 1999c.

Woo, R., and J.M. Martin, Source regions of the slow solar wind, *Geophys. Res. Lett.*, *24*, 2535–2538, 1997.

Yokobe, A., T. Ohmi, K. Hakamada, M. Kojima, M. Tokumaru, B.V. Jackson, P.P. Hick, and S. Zidowitz, in *Solar Wind Nine*, eds. S.R. Habbal, R. Esser, J.V. Hollweg, and P. Isenberg, 565–567, AIP, New York, 1999.

Zhao, X.P., and A.J. Hundhausen, Organization of solar wind plasma properties in a tilted, heliomagnetic coroordinate system, *J. Geophys. Res.*, *86*, 5423–5430, 1981.

Zirker, J., *Coronal Holes and High Speed Streams*, ed. J.B. Zirker, Colorado Associated University Press, Colorado, 1977.

FIGURE CAPTIONS

Plate 1. Observations during the period of 17–21 January 1997. (a) White light image of the corona taken with the LASCO C2 coronagraph on SOHO on 1997 January 17. The white contours mark the ratio of the oxygen 1032/1037 line intensities equal to 2, or equivalently 94 km s^{-1} [*Habbal et al.*, 1997]. The dashed white lines demarcate the streamer, quiet Sun, and polar coronal hole regions, and are correspondingly shown as vertical lines in (b)–(d). Profile of radial distance to 94 km s^{-1} contour in (a) is shown in (b)–(d). The Mk III pB profile at 1.15 Ro is combined in (b), while the Mk III pB profile at 1.74 Ro is combined in (c). The horizontal line in (c) corresponds to $pB = 100 \times 10^{-10}$ Bo.

Plate 2. Same as Plate 1 except for observations during the period of 23–27 April 1997.

Plate 3. (a) Solar wind flow speed contours constructed by *Neugebauer et al.* [1998] from solar wind measurements by Ulysses and WIND during Carrington rotations CR 1891–1895; superimposed is the Mk III synoptic map of pB contours (10^{-10} Bo) at 1.74 Ro for CR 1893 based on east limb measurements. Note that in all of the Mk III synoptic maps in this figure, the 100 contour level is that between 50 and 200. (b) Same as (a) except the pB contours are for CR 1891 and are based on west limb measurements.

Plate 4. (a) Solar wind speed maps determined during CR 1857–1858 using tomographic reconstruction of IPS measurements made with the Nagoya network of radio telescopes in the distance range of 0.3–1.0 AU [*Kojima et al.*, 1998]; superimposed is the Mk III synoptic map of pB contours at 1.74 Ro based on west limb data during CR 1857. (b) Same as (a) except the IPS map is for CR 1912 and the synoptic map of pB at 1.74 Ro is based on east limb data during CR 1912.

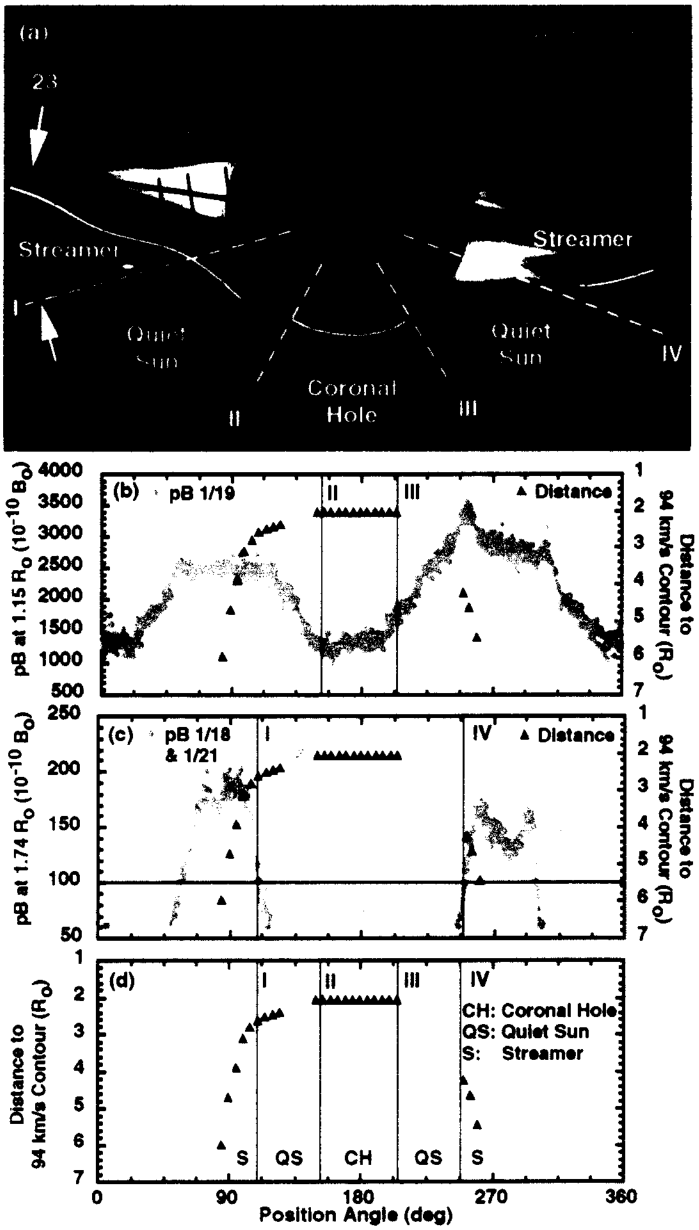
(a)
23
Streamer
Streamer
I
II
III
IV
Quiet Sun
Quiet Sun
Coronal Hole
(b) pB 1/19
▲ Distance
pB at 1.15 R$_o$ (10^{-10} B$_o$)
4000
3500
3000
2500
2000
1500
1000
500
Distance to 94 km/s Contour (R$_o$)
1
2
3
4
5
6
7
(c) pB 1/18 & 1/21
▲ Distance
pB at 1.74 R$_o$ (10^{-10} B$_o$)
250
200
150
100
50
(d)
CH: Coronal Hole
QS: Quiet Sun
S: Streamer
S
QS
CH
QS
S
0
90
180
270
360
Position Angle (deg)

Plate

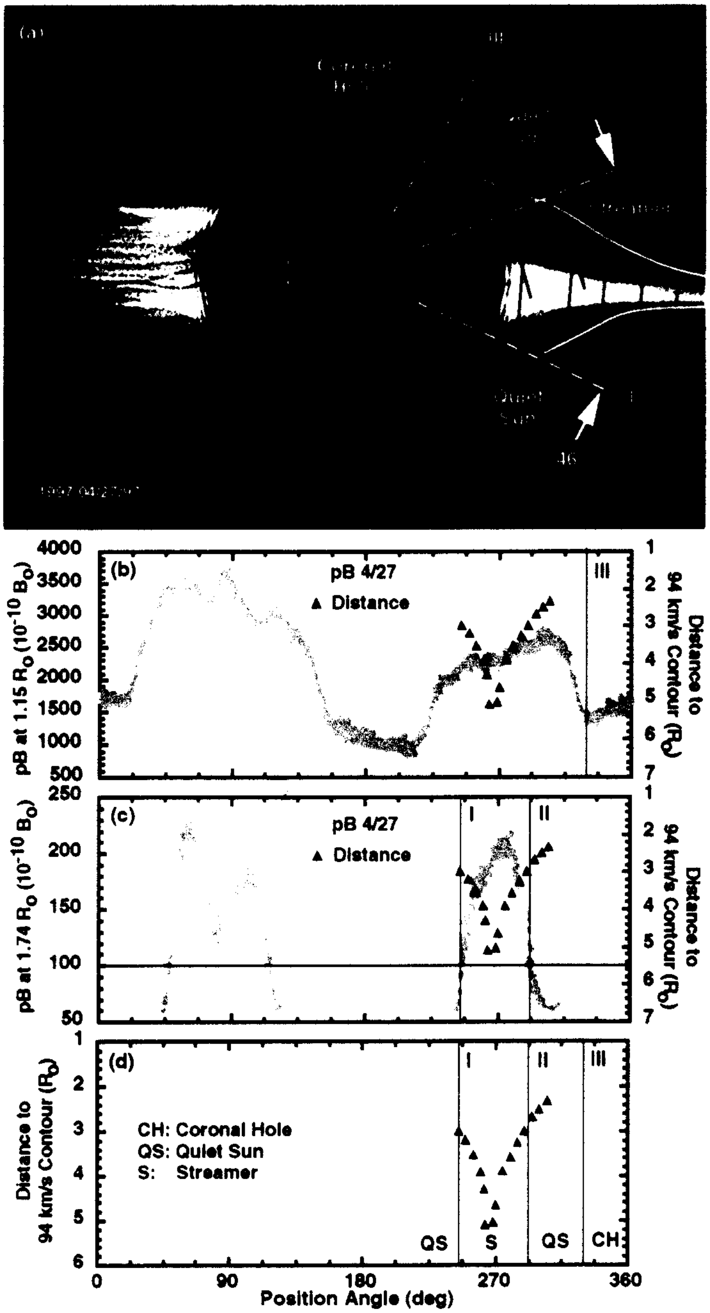
(a)
III
Coronal Hole
Streamer
Quiet Sun
I
46
1997 04 27
(b)
pB 4/27
▲ Distance
III
pB at 1.15 R_O (10^{-10} B_O)
4000
3500
3000
2500
2000
1500
1000
500
Distance to 94 km/s Contour (R_O)
1
2
3
4
5
6
7
(c)
pB 4/27
▲ Distance
I
II
pB at 1.74 R_O (10^{-10} B_O)
250
200
150
100
50
(d)
I
II
III
Distance to 94 km/s Contour (R_O)
CH: Coronal Hole
QS: Quiet Sun
S: Streamer
QS
S
QS
CH
0
90
180
270
360
Position Angle (deg)

Plate

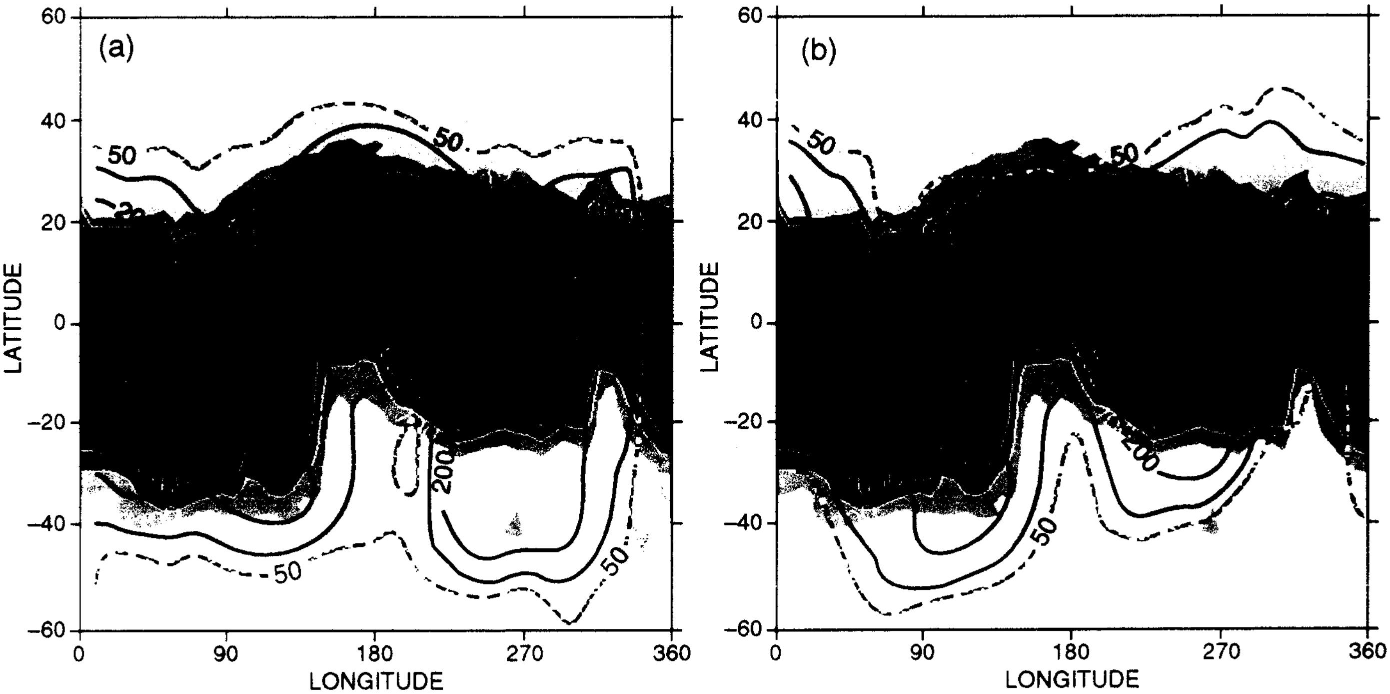

Plate 3

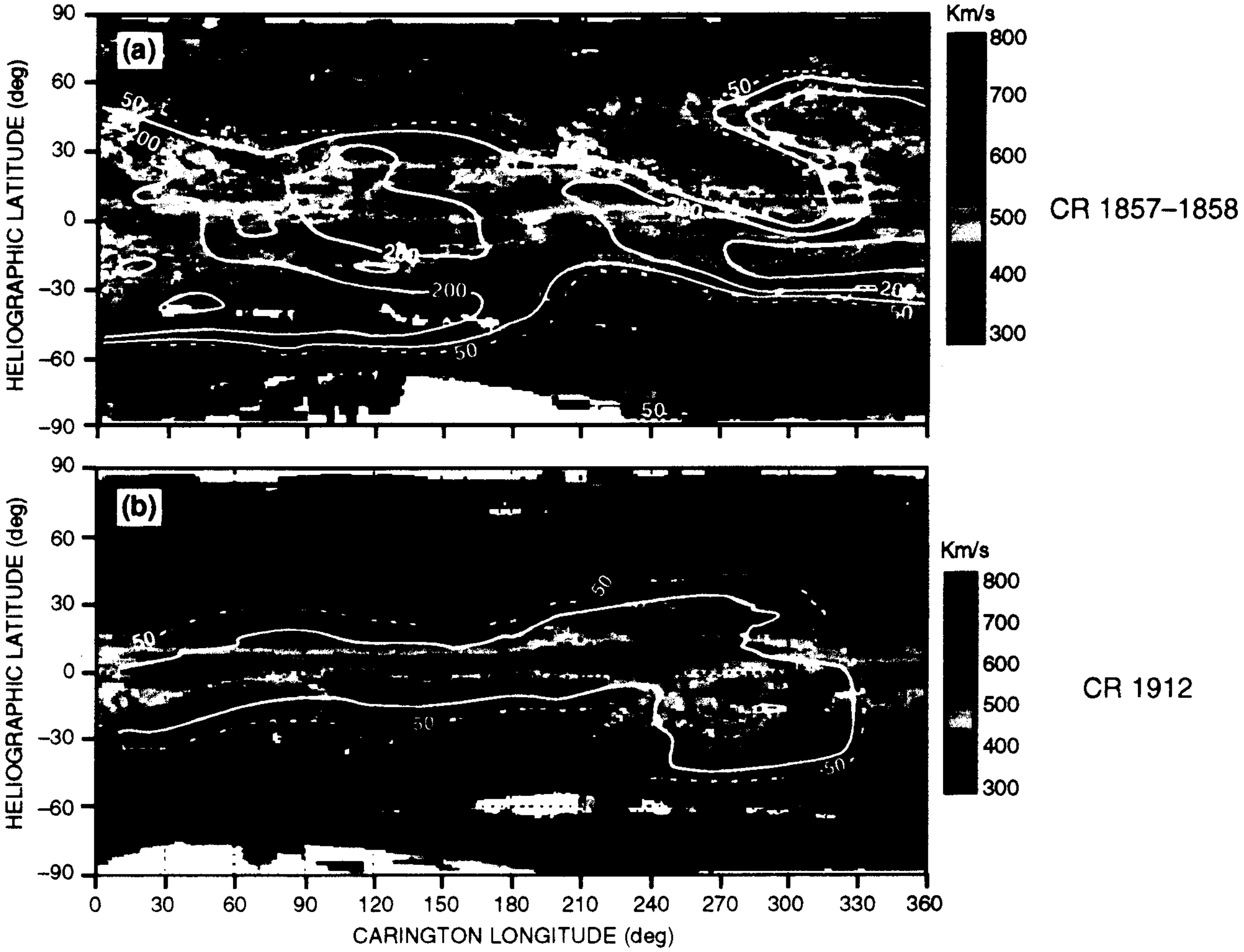
(a)
(b)
HELIOGRAPHIC LATITUDE (deg)
90
60
30
0
-30
-60
-90
50
200
Km/s
800
700
600
500
400
300
CR 1857–1858
CR 1912
0
30
60
90
120
150
180
210
240
270
300
330
360
CARINGTON LONGITUDE (deg)

Plate